Chemistry of Metals and Alloys

Chem. Met. Alloys 15 (2022) 35-43
Ivan Franko National University of Lviv
www.chemetal-journal.org

The Mo–Pd–Ge system at 600°C

Bohdan KOROTOSHYN[1]*, Nataliya MUTS[1], Yaroslav TOKAYCHUK[1], Roman GLADYSHEVSKII[1]

[1]*Department of Inorganic Chemistry, Ivan Franko National University of Lviv, Kyryla i Mefodiya St. 6, UA-79005 Lviv, Ukraine*
* *Corresponding author. E-mail:* Bohdan.Korotoshyn@lnu.edu.ua

Received October 15, 2022; accepted December 28, 2022
https://doi.org/10.30970/cma15.0430

The isothermal cross-section of the phase diagram of the ternary Mo–Pd–Ge system at 600°C was constructed based on X-ray diffraction and energy-dispersive X-ray spectroscopy. The formation of solid solutions based on the binary compound $MoGe_2$ with structure type $PbCl_2$ (Pearson symbol *oP*12, space group *Pnma*) and the binary compound PdGe with structure type FeAs (*oP*8, *Pnma*) was established.

Phase equilibria / Palladium / Molybdenum / Germanium / Solid solution

1. Introduction

The purpose of the work was to study the phase equilibria in the Mo–Pd–Ge system at 600°C. As objects of research we chose palladium, a metal with unique catalytic properties, molybdenum, which is characterized by high hardness, and germanium – a typical semi-metal. A comparison of the three metals shows that molybdenum has the highest melting point, palladium the highest density and electronegativity, and germanium the largest atomic radius.

Palladium has the widest range of applications among the abovementioned metals. The largest domains of application are mechanical engineering and electronics, as well as medicine and jewelry. However, palladium is best known in chemistry as a universal catalyst in many chemical processes. Catalysts based on intermetallic palladium compounds are becoming increasingly used for reactions of oil cracking, or hydrogenation and dehydrogenation of organic compounds. For instance, the catalytic activity of the composite $GaPd_2/SiO_2$ on the synthesis of methanol from carbon dioxide and hydrogen makes it possible to carry out the process at much lower pressures and temperatures than with the usual catalyst $Cu/ZnO/Al_2O_3$ [1]. The compound $Pd_2Ga_{0.85}Sb_{0.15}$ is another example of the catalytic activity of palladium alloys. It shows high activity and selectivity in the semi-hydrogenation of acetylene with excess of ethylene [2]. Hence, the study of the catalytic properties of palladium-based alloys is relevant and needed for many chemical processes in industry and chemical synthesis.

The better catalytic activity of intermetallic compounds in hydrogenation processes, compared with pure palladium, is explained by the unique mechanism of the reactions. For example, in the semi-hydrogenation reaction of acetylene to ethylene, when a pure metal catalyst is used, the close arrangement of palladium atoms relative to each other significantly complicates the isolation of atoms and the formation of active centers. As a result, strong di-σ-bonding is present, which leads to the formation of a considerable amount of unwanted ethane. In intermetallic compounds there is a decrease in the number of Pd–Pd bonds in the crystal structures of the compounds, accompanied by an increase of the interatomic distances. Consequently, palladium compounds in which the active centers are properly isolated, have weak π-binding of the acetylene molecule to the palladium atom. This makes it possible to increase both the selectivity of the reaction and the yield of the product. In addition, the introduction into the system of less electronegative elements than palladium leads to a transfer of partially negative charge to the Pd atom and greater filling of its *d*-orbitals in the electronic configuration. Increasing the energy of the active centers greatly improves the absorption properties of palladium. In addition, the use of palladium alloys as catalysts makes it possible, not only to increase the efficiency of the process, but also to reduce its cost by reducing the consumption of precious metal.

The binary Mo–Pd, Pd–Ge, and Mo–Ge systems have been well studied [3] (Table 1). According to the Pauling File [3] the extended solubility of Mo in Pd reaches its maximum of 57 at.% at 1700°C. The maximum solubility of Pd in Mo is 7 at.% at 1755°C. Two compounds are formed in the Mo–Pd system [4,5] (Table 1): $MoPd_2$ (structure type $MoPt_2$, Pearson symbol *oI*6, space group *Immm*) and $Mo_{0.5}Pd_{0.5}$ (Mg, *hP*2, $P6_3/mmc$). Both compounds have certain homogeneity regions. The binary $Mo_{0.5}Pd_{0.5}$ compound exists in a narrow temperature range (1370-1755°C).

According to the phase diagram of the Mo–Ge system [3], the solubility of Ge in Mo reaches 6 at.% at 1800°C, while Mo is practically insoluble in Ge. In the Mo–Ge binary system in the temperature range from 800 to 2600°C, four compounds are formed [6-10] (Table 1): $MoGe_2$ ($PbCl_2$, *oP*12, *Pnma*), $Mo_{13}Ge_{23}$ ($Mo_{13}Ge_{23}$, *tP*144, *P*-4*n*2), Mo_5Ge_3 (W_5Si_3, *tI*32, *I4/mcm)*, Mo_3Ge (Cr_3Si, *cP*8, *Pm*-3*n)*. Brown [7] confirmed the existence in the system of a high-pressure modification of the binary compound $MoGe_2$ ($MoSi_2$, *tI*6, *I4/mmm*) and the compound $MoGe_{1.7}$ (space group $I4_122$).

The maximum solubility of Ge in Pd (3 at.%) is observed in the temperature range between 775 and 840°C, while Pd is practically insoluble in Ge. According to the Pauling File [3], seven binary compounds are known in the Pd–Ge system in the temperature range from 200 to 1600°C [11-16] (Table 1): PdGe (FeAs, *oP*8, *Pnma*), Pd_2Ge (Fe_2P, *hP*9, *P*-62*m*), $Pd_{21}Ge_8$ (Pt_8Al_{21}, *tI*116, $I4_1/a$), $Pd_{25}Ge_9$ ($Pd_{25}Ge_9$, *hP*34, *P*-3), Pd_3Ge (structure not identified), Pd_5Ge (Pd_5As, *mS*24, *C*2), $Pd_{0.84}Ge_{0.16}$ (W, *cI*2, *Im*-3*m*).

2. Experimental details

Two binary and 13 ternary alloys were prepared by arc-melting the elements under a purified argon atmosphere. Elements of the following purities were used: Pd, 99.95 mass%; Mo, 99.8 mass%; Ge, 99.98 mass%. The samples were annealed at 600°C for 150 days in evacuated quartz tubes, and subsequently quenched in cold water. The mass of each sample was approximately 1 g. Phase analysis and determination of the crystal structures of the phases were carried out based on X-ray powder diffraction patterns, recorded with a DRON-2.0 M diffractometer (Fe *K*α radiation), a HZG-4a diffractometer (Cu *K*α radiation), or a STOE Stadi P diffractometer (Cu $K\alpha_1$ radiation), using the program package FullProf Suite [17]. Energy-dispersive X-ray spectroscopy (EDS), using an X-MaxN microanalysis system and a scanning electron microscope (SEM) Tescan Vega 3, was used to confirm the elemental composition of the samples. The compositions of the individual phases present in the sample were determined by EDS analysis using AZtecLive real-time chemical imaging powered by an X-MaxN Silicon Drift Detector.

3. Results and discussion

3.1. Energy-dispersive X-ray spectroscopy

Sample $Mo_{10}Pd_{25}Ge_{65}$. The composition of the sample according to the results of energy-dispersive X-ray spectroscopy is $Pd_{12.56}Mo_{28.67}Ge_{58.77}$. The sample $Mo_{10}Pd_{25}Ge_{65}$ contains three phases: light gray spots on the surface image corresponds to the binary compound Pd_2Ge [$Pd_{67(1)}Ge_{33(1)}$]; the dim gray matrix is a solid solution of Mo in the binary compound PdGe [$Pd_{42.4}Mo_{6.8}Ge_{50.8}$]; the dark areas correspond to the phase $MoGe_2$ [$Pd_{2.32(54)}Mo_{33.99(52)}Ge_{63.69(10)}$] (Fig. 1).

Sample $Pd_{20}Mo_{60}Ge_{20}$. The composition of the sample $Pd_{24.91}Mo_{57.17}Ge_{17.92}$ determined by EDS agrees with the nominal composition of the sample ($Pd_{20}Mo_{60}Ge_{20}$). The sample $Pd_{20}Mo_{60}Ge_{20}$ contains three phases: the light gray matrix corresponds to the binary compound Pd_2Ge [$Pd_{69.0(1)}Mo_{1(1)}Ge_{30(1)}$]; the dim gray area to the solid solution of Mo [$Pd_{1.3(7)}Mo_{92.7(5)}Ge_{6.0(4)}$]; the dark regions at the edge of the two abovementioned phases to the binary compound Mo_3Ge.

Table 1 Crystallographic data for known binary compounds in the Mo–Pd, Mo–Ge and Pd–Ge systems.

Compound	Structure type	Pearson symbol	Space group	Cell parameters, Å			Reference
				a	*b*	*c*	
$MoPd_2$	$MoPt_2$	*oI*6	*Immm*	2.75	3.89	8.25	[4]
$Mo_{0.5}Pd_{0.5}$	Mg	*hP*2	$P6_3/mmc$	2.777	–	4.490	[5]
$MoGe_2$	$MoSi_2$	*tI*6	*I4/mmm*	3.322	–	8.219	[6]
$MoGe_2$	$PbCl_2$	*oP*12	*Pnma*	6.343	3.451	8.582	[7]
$Mo_{13}Ge_{23}$	$Mo_{13}Ge_{23}$	*tP*144	*P*-4*n*2	5.987	–	63.54	[8]
Mo_5Ge_3	W_5Si_3	*tI*32	*I4/mcm*	9.845	–	4.965	[9]
$MoGe_{1.7}$	unidentified		$I4_122$	5.944	–	44.3995	[7]
Mo_3Ge	Cr_3Si	*cP*8	*Pm*-3*n*	4.93	–	–	[10]
PdGe	FeAs	*oP*8	*Pnma*	5.782	3.481	6.259	[11]
Pd_2Ge	Fe_2P	*hP*9	*P*-62*m*	6.712	–	3.408	[12]
$Pd_{21}Ge_8$	Pt_8Al_{21}	*tI*116	$I4_1/a$	13.067	–	10.033	[13]
$Pd_{25}Ge_9$	$Pd_{25}Ge_9$	*hP*34	*P*-3	7.351	–	10.605	[14]
Pd_3Ge	unknown structure						[3]
Pd_5Ge	Pd_5As	*mS*24	*C*2	5.509	7.725	8.375	[15]
$Pd_{0.84}Ge_{0.16}$	W	*cI*2	*Im*-3*m*	3.085	–	–	[16]

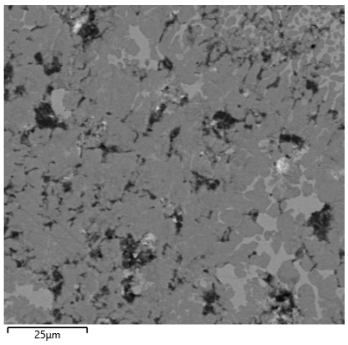

a) **$Mo_{10}Pd_{25}Ge_{65}$**

light gray spots – $[Pd_{67(1)}Ge_{33(1)}]$, Pd_2Ge (type Fe_2P);

dim gray matrix – $[Pd_{42.4(2)}Mo_{6.8(1)}Ge_{50.8(2)}]$, $(Pd_{0.86}Mo_{0.14})Ge$ (FeAs);

dark areas – $[Pd_{2.3(5)}Mo_{34.0(5)}Ge_{63.7(1)}]$, $MoGe_2$ ($PbCl_2$).

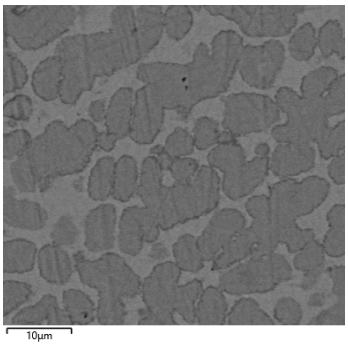

b) **$Pd_{20}Mo_{60}Ge_{20}$**

light gray matrix – $[Pd_{69.0(1)}Mo_{1(1)}Ge_{30(1)}]$, Pd_2Ge (type Fe_2P);

dim gray area – $[Pd_{1.3(7)}Mo_{92.7(5)}Ge_{6.0(4)}]$, Mo (W);

dark regions at the edge of the two abovementioned phases – Mo_3Ge (Cr_3Si).

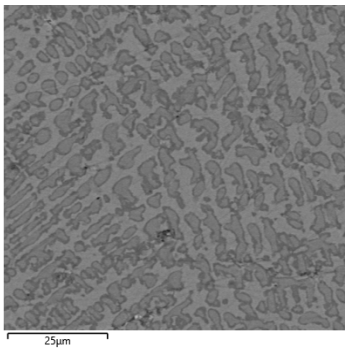

c) **$Pd_{30}Mo_{30}Ge_{40}$**

light gray matrix – $[Pd_{68.0(7)}Mo_{0.3(2)}Ge_{31.7(5)}]$, Pd_2Ge (type Fe_2P);

dim gray area – $[Pd_{1.1(1)}Mo_{73.8(1)}Ge_{25.1(1)}]$, Mo_3Ge (Cr_3Si);

dark regions at the edge of the two abovementioned phases – $[Pd_{10(1)}Mo_{33(1)}Ge_{57(1)}]$, $MoGe_2$ ($PbCl_2$).

Fig. 1 Results of the EDS investigation of the phase compositions of the $Mo_{10}Pd_{25}Ge_{65}$, $Pd_{20}Mo_{60}Ge_{20}$, and $Pd_{30}Mo_{30}Ge_{40}$ samples.

Sample $Pd_{30}Mo_{30}Ge_{40}$. According to the EDS results, the composition of the sample is $Pd_{33.67}Mo_{28.79}Ge_{37.54}$. The sample $Pd_{30}Mo_{30}Ge_{40}$ contains three phases: the light gray matrix corresponds to the binary compound Pd_2Ge $[Pd_{67.0(7)}Mo_{0.3(7)}Ge_{34.7(7)}]$; the dim gray area to the binary compound Mo_3Ge $[Pd_{1.1(1)}Mo_{73.8(1)}Ge_{25.1(1)}]$. The dark regions at the edge of the two abovementioned phases are considered to be the solid solution of Pd in the binary compound $MoGe_2$ $[Pd_{10(1)}Mo_{33(1)}Ge_{57(1)}]$ (Fig. 1).

3.2. X-ray phase analysis

The isothermal cross-section of the phase diagram of the ternary Mo–Pd–Ge system at 600°C was constructed based on the results of X-ray diffraction and energy-dispersive X-ray spectroscopy of the 15 alloys (Fig. 2). Two binary samples ($Mo_{38}Ge_{62}$ and $Mo_{63}Ge_{37}$) and a sample with low palladium content ($Mo_{58}Pd_5Ge_{37}$) were synthesized in order to confirm the existence of the binary compounds Mo_5Ge_3 and $Mo_{13}Ge_{23}$.

The binary compounds Mo_5Ge_3 with W_5Si_3 structure type and $Mo_{13}Ge_{23}$ with own structure type were not detected in other ternary samples due to the phase equilibrium Mo_3Ge – $(Mo_{0.87}Pd_{0.13})Ge_2$ – Pd_2Ge implying the formation of a solid solution based on the binary compound $MoGe_2$.

The small amount of Pd in the sample $Mo_{58}Pd_5Ge_{37}$ could be dissolved in either the Mo_3Ge or the Mo_5Ge_3 binary compounds. Attempts to study the palladium-rich region were unsuccessful and the compositions of the samples $Mo_{10}Pd_{75}Ge_{15}$, $Mo_{10}Pd_{80}Ge_{10}$, and $Mo_{20}Pd_{65}Ge_{15}$ turned out to be in the Mo – Mo_3Ge – Pd_2Ge region.

Based on the results of X-ray powder diffraction and EDS, we could confirm the existence of the following binary compounds: $MoGe_2$ (structure type $PbCl_2$, Pearson symbol *oP*12, space

group *Pnma*), Mo_3Ge (Cr_3Si, *cP*8, *Pm*-3*n*), PdGe (FeAs, *oP*8, *Pnma*), Pd_2Ge (Fe_2P, *hP*9, *P*-62*m*), Mo_5Ge_3 (W_5Si_3, *tI*32, *I*4/*mcm*), and $Mo_{13}Ge_{23}$ ($Mo_{13}Ge_{23}$, *tP*144, *P*-4*n*2). The unit-cell parameters were refined for the individual binary phases (Table 2).

We have constructed the isothermal cross-section of the phase diagram of the ternary Mo–Pd–Ge system at 600°C and established the existence of the following five three-phase equilibria (Fig. 2):
Mo_5Ge_3 – $Mo_{13}Ge_{23}$ – $(Mo_{0.87}Pd_{0.13})Ge_2$,
Mo – Mo_3Ge – Pd_2Ge,
Mo_3Ge – $(Mo_{0.87}Pd_{0.13})Ge_2$ – Pd_2Ge,
$(Mo_{0.87}Pd_{0.13})Ge_2$ – $(Mo_{0.14}Pd_{0.86})Ge$ – Pd_2Ge,
$(Mo_{0.87}Pd_{0.13})Ge_2$ – $(Mo_{0.14}Pd_{0.86})Ge$ – Ge.

Table 2 Phase composition of samples of the Mo–Pd–Ge system at 600°C and unit-cell parameters of the individual phases.

Sample	Phase, structure type, Pearson symbol, space group	Content (wt.%)	Unit-cell parameters (Å)
$Mo_{38}Ge_{62}$	Mo_5Ge_3, W_5Si_3, *tI*32, *I*4/*mcm*	88(2)	*a* =9.8469(4), *c* = 4.9812(3)
	$Mo_{13}Ge_{23}$, $Mo_{13}Ge_{23}$, *tP*144, *P*-4*n*2	12(1)	*a* = 5.993(5), *c* = 63.75(6)
$Mo_{63}Ge_{37}$	Mo_3Ge, Cr_3Si, *cP*8, *Pm*-3*n*	84(2)	*a* = 4.9514(7)
	Mo_5Ge_3, W_5Si_3, *tI*32, *I*4/*mcm*	16(1)	*a* =9.815(9), *c* = 5.050(6)
$Mo_{10}Pd_{25}Ge_{65}$	$(Mo_{0.87}Pd_{0.13})Ge_2$, $PbCl_2$, *oP*12, *Pnma*	78(3)	*a* = 6.348(1), *b* = 3.4538(6), *c* = 8.585(1)
	$(Mo_{0.14}Pd_{0.86})Ge$, FeAs, *oP*8, *Pnma*	15(1)	*a* = 6.290(3), *b* = 3.482(1), *c* = 5.806(2)
	Pd_2Ge, Fe_2P, *hP*9, *P*-62*m*	7(1)	*a* = 6.724(3), *c* = 3.419(2)
$Mo_{10}Pd_{10}Ge_{80}$	$(Mo_{0.87}Pd_{0.13})Ge_2$, $PbCl_2$, *oP*12, *Pnma*	63(1)	*a* = 6.349(1), *b* = 3.4556(8), *c* = 8.588(2)
	$(Mo_{0.14}Pd_{0.86})Ge$, FeAs, *oP*8, *Pnma*	30(1)	*a* = 6.287(2), *b* = 3.4956(8), *c* = 5.807(1)
	Ge, C, *cF*8, *Fd*-3*m*	7(1)	*a* = 5.6644(9)
$Mo_{10}Pd_{75}Ge_{15}$	Pd_2Ge, Fe_2P, *hP*9, *P*-62*m*	88(2)	*a* = 6.716, *c* = 3.4027
	Mo_3Ge, Cr_3Si, *cP*8, *Pm*-3*n*	12(2)	*a* = 4.942
$Mo_{10}Pd_{80}Ge_{10}$	Pd_2Ge, Fe_2P, *hP*9, *P*-62*m*	89(1)	*a* = 6.7055(4), *c* = 3.4028(3)
	Mo_3Ge, Cr_3Si, *cP*8, *Pm*-3*n*	11(1)	*a* = 4.9309(6)
$Mo_{20}Pd_{50}Ge_{30}$	Pd_2Ge, Fe_2P, *hP*9, *P*-62*m*	65(2)	*a* = 6.727(2), *c* = 3.420(1)
	$(Mo_{0.87}Pd_{0.13})Ge_2$, $PbCl_2$, *oP*12, *Pnma*	23(2)	*a* = 6.356(5), *b* = 3.452(3), *c* = 8,608(6)
	Mo_3Ge, Cr_3Si, *cP*8, *Pm*-3*n*	12(1)	*a* = 4.949(2)
$Mo_{20}Pd_{65}Ge_{15}$	Pd_2Ge, Fe_2P, *hP*9, *P*-62*m*	76(2)	*a* = 6.733(2), *c* = 3.417(1)
	Mo_3Ge, Cr_3Si, *cP*8, *Pm*-3*n*	24(1)	*a* = 4.9453(9)
$Mo_{21}Pd_{16.5}Ge_{62.5}$	$(Mo_{0.87}Pd_{0.13})Ge_2$, $PbCl_2$, *oP*12, *Pnma*	80(2)	*a* = 6.344(1), *b* = 3.4511(6), *c* = 8.584(2)
	$(Mo_{0.14}Pd_{0.86})Ge$, FeAs, *oP*8, *Pnma*	15(1)	*a* = 6.290(3), *b* = 3.474(1), *c* = 5.814(3)
	Pd_2Ge, Fe_2P, *hP*9, *P*-62*m*	5(1)	*a* = 6.723(4), *c* = 3.417(3)
$Mo_{30}Pd_{30}Ge_{40}$	Pd_2Ge, Fe_2P, *hP*9, *P*-62*m*	43.0(4)	*a* = 6.7126(6), *c* = 3.4053(4)
	$(Mo_{0.87}Pd_{0.13})Ge_2$, $PbCl_2$, *oP*12, *Pnma*	38.8(6)	*a* = 6.3424(4), *b* = 3.4507(2), *c* = 8,5841(5)
	Mo_3Ge, Cr_3Si, *cP*8, *Pm*-3*n*	18.2(2)	*a* = 4.9364(3)
$Mo_{33.6}Pd_{3.6}Ge_{62.8}$	$(Mo_{0.87}Pd_{0.13})Ge_2$, $PbCl_2$, *oP*12, *Pnma*	96(3)	*a* = 6.3461(8), *b* = 3.4523(4), *c* = 8.5861(9)
	Pd_2Ge, Fe_2P, *hP*9, *P*-62*m*	4(1)	*a* = 6.712, *c* = 3.408
$Mo_{50}Pd_{35}Ge_{15}$	Pd_2Ge, Fe_2P, *hP*9, *P*-62*m*	40(1)	*a* = 6.713(2), *c* = 3.401(1)
	Mo_3Ge, Cr_3Si, *cP*8, *Pm*-3*n*	32(1)	*a* = 4.9363(5)
	Mo, W, *cI*2, *Im*-3*m*	28(1)	*a* = 3.1515(2)
$Mo_{58}Pd_5Ge_{37}$	Mo_3Ge, Cr_3Si, *cP*8, *Pm*-3*n*	59(1)	*a* = 4.9434(3)
	Mo_5Ge_3, W_5Si_3, *tI*32, *I*4/*mcm*	41(1)	*a* =9.859(1), *c* = 4.9902(9)
$Mo_{60}Pd_{20}Ge_{20}$	Mo, W, *cI*2, *Im*-3*m*	50(2)	*a* = 3.1413(2)
	Mo_3Ge, Cr_3Si, *cP*8, *Pm*-3*n*	18(1)	*a* = 4.9383(3)
	Pd_2Ge, Fe_2P, *hP*9, *P*-62*m*	32(2)	*a* = 6.7089(8), *c* = 3.4043(5)
$Mo_{80}Pd_{10}Ge_{10}$	Mo, W, *cI*2, *Im*-3*m*	78(2)	*a* = 3.1482(4)
	Pd_2Ge, Fe_2P, *hP*9, *P*-62*m*	17(1)	*a* = 6.713(4), *c* = 3.411(3)
	Mo_3Ge, Cr_3Si, *cP*8, *Pm*-3*n*	5(1)	*a* = 4.940(3)

Note: $(Mo_{0.87}Pd_{0.13})Ge_2$ – solid solution based on the binary $MoGe_2$ compound; $(Mo_{0.14}Pd_{0.86})Ge$ – solid solution based on the binary PdGe compound.

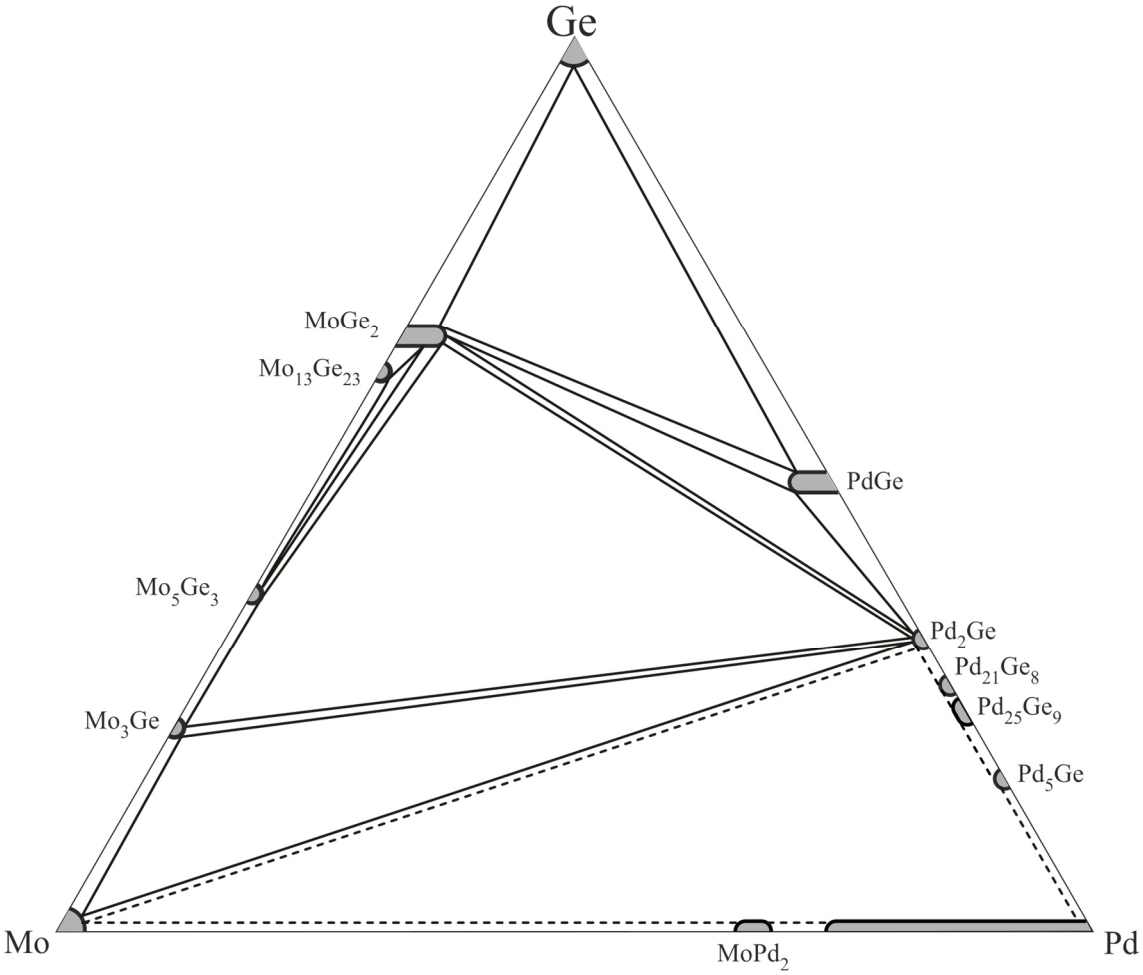

Fig. 2 The isothermal cross-section of the Mo–Pd–Ge system at 600°C.

3.3. X-ray structure analysis

The structure of the solid solution based on the binary $MoGe_2$ compound was refined on diffraction data from a polycrystalline sample of composition $Mo_{30}Pd_{30}Ge_{40}$. The refinements were carried out with the full-profile Rietveld method. Cell parameters and atomic coordinates for the initial model were taken from the compound $MoGe_2$ [7]. The refinement of the crystal structure showed that one of the sites in Wyckoff position 4*c* of the space group *Pnma* is occupied by a statistical mixture of palladium and molybdenum atoms. The powder diffraction pattern is shown in Fig. 3 and experimental details of the Rietveld refinement are given in Table 3. Three phases were observed: 43.0(4) wt.% of Pd_2Ge with hexagonal Fe_2P-type structure (*hP*9, *P*-62*m*), 38.8(6) wt.% of the $(Mo_{0.87}Pd_{0.13})Ge_2$ phase with structure type $PbCl_2$ (*oP*12, *Pnma*), and 18.2(2) wt.% of Mo_3Ge with cubic Cr_3Si-type structure (*cP*8, *Pm*-3*n*).

The atomic coordinates for the $(Mo_{0.87}Pd_{0.13})Ge_2$ phase, and the binary Mo_5Ge_3 and Pd_2Ge compounds, presented in Table 4, are in good agreement with literature data. Powder diagrams for the $Mo_{38}Ge_{62}$, $Mo_{10}Pd_{25}Ge_{65}$, $Mo_{10}Pd_{80}Ge_{10}$, and $Mo_{33.6}Pd_{3.6}Ge_{62.8}$ samples are shown in Fig. 4.

Projections of the crystal structure of the $(Mo_{0.87}Pd_{0.13})Ge_2$ phase and the coordination polyhedra of the atoms are presented on Fig. 5. The atoms of Ge are shown in blue, and the statistical mixture of Mo and Pd in red. The coordination number for the atom site Ge1 is 8 $[(Mo_{0.87}Pd_{0.13})_4Ge_4]$, for Ge2 it is 7 $[(Mo_{0.87}Pd_{0.13})_4Ge_3]$, whereas the largest coordination number is observed for the statistical mixture of Mo and Pd atoms – 9 $[Ge_9]$ (Table 5). From the analysis of the crystal structure of the solid solution $(Mo_{0.87}Pd_{0.13})Ge_2$ (Fig. 5) we can assume that the arrangement of the statistical Mo/Pd mixture favors the formation of active centers on the surface thanks to Ge atom nets that isolate the atoms of the statistic mixture $(Mo_{0.87}Pd_{0.13})$ from each other.

Table 3 Experimental details of the structure refinement of the $Mo_{30}Pd_{30}Ge_{40}$ sample.

Phase	Pd_2Ge	$(Mo_{0.87}Pd_{0.13})Ge_2$	Mo_3Ge
Content, mass%	43.0(4)	38.8(6)	18.2(2)
Structure type	Fe_2P	$PbCl_2$	Cr_3Si
Pearson symbol	*hP*9	*oP*12	*cP*8
Space group	*P*-62*m*	*Pnma*	*Pm*-3*n*
Unit-cell parameters:			
a (Å)	6.7126(6)	6.3424(4)	4.9364(3)
b (Å)	–	3.4507(2)	–
c (Å)	3.4053(4)	8.5841(6)	–
Cell volume *V* (Å^3)	132.88(2)	187.87(2)	120.29(1)
Formula units per cell *Z*	3	4	2
Density D_x (g cm^{-3})	10.699	8.573	9.951
Preferred orientation [direction]	–	0.951(4) [010]	–
Reliability factors:			
R_B	6.00	7.98	3.98
R_F	3.80	6.94	4.57
Profile parameters:			
U		0.041(7)	
V		0.005(7)	
W		0.010(2)	
Asymmetry parameters		0.04(2) 0.005(4)	
Reliability factors:			
R_p		8.86	
R_{wp}		12.0	
χ^2		2.13	

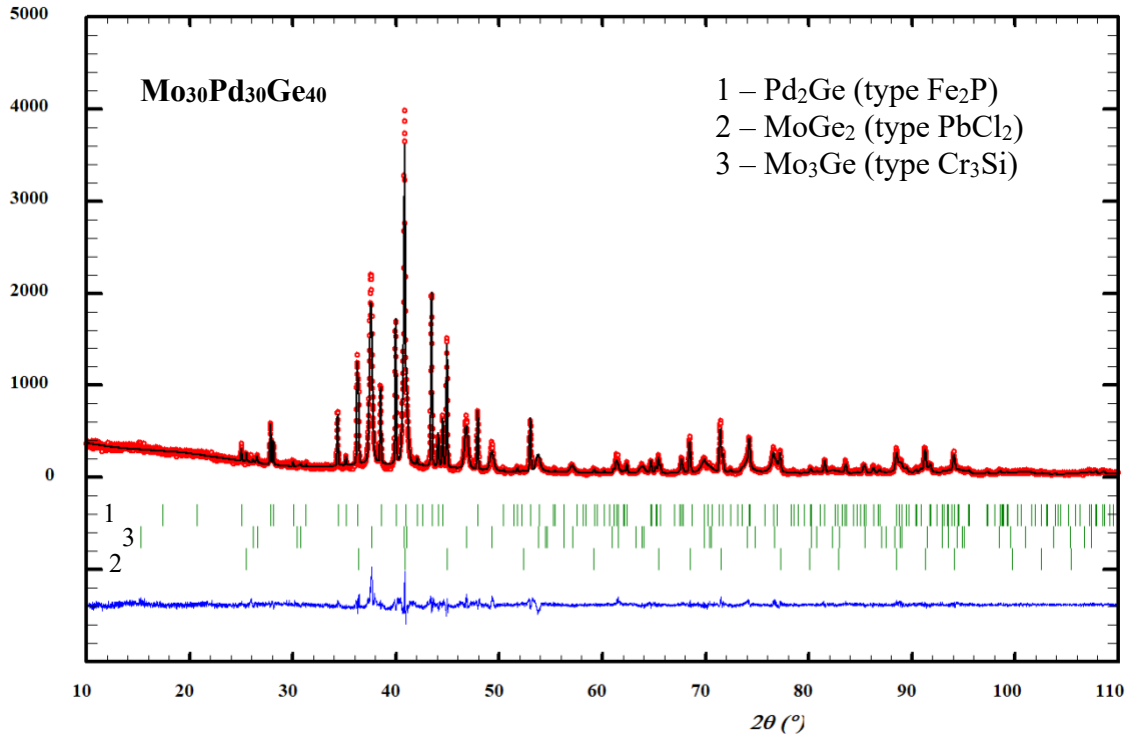

Fig. 3 Observed, calculated and difference (bottom) X-ray powder diffraction patterns for the $Mo_{30}Pd_{30}Ge_{40}$ sample annealed at 600°C for 150 days; Cu $K\alpha_1$ radiation (Pd_2Ge – 43.0(4) wt.%, structure type Fe_2P; $MoGe_2$ – 38.8(6) wt.%, structure type $PbCl_2$; Mo_3Ge – 18.2(2) wt.%, structure type Cr_3Si).

Table 4 Atomic coordinates for the $(Mo_{0.87}Pd_{0.13})Ge_2$ phase and the binary Mo_5Ge_3 and Pd_2Ge compounds.

$(Mo_{0.87}Pd_{0.13})Ge_2$ ($PbCl_2$, *oP*12, *Pnma*), a = 6.3424(4), b = 3.4507(2), c = 8.5841(6) Å, Z = 4						
Atom	Wyckoff position	Atomic coordinates			Occupancy	B_{iso} (Å^2)
		x	*y*	*z*		
Mo	4*c*	0.2502(5)	1/4	0.3273(4)	0.87(5)	0.85(7)
Pd	4*c*	0.2502(5)	1/4	0.3273(4)	0.13(5)	0.85(7)
Ge1	4*c*	0.1391(6)	1/4	0.0399(5)	1	1.0(1)
Ge2	4*c*	0.0652(6)	1/4	0.6355(5)	1	1.1(1)
Mo_5Ge_3 (W_5Si_3, *tI*32, *I4/mcm*), a = 9.8469(4), c = 4.9812(3) Å, Z = 4						
Atom	Wyckoff position	Atomic coordinates				B_{iso} (Å^2)
		x	*y*	*z*		
Mo1	16*k*	0.0776(6)	0.2268(6)	0		0.48(9)
Mo2	4*b*	0	1/2	1/4		0.48(9)
Ge1	8*h*	0.1701(8)	0.6701(8)	0		0.86(10)
Ge2	4*a*	0	0	1/4		0.86(10)
Pd_2Ge (Fe_2P, *hP*9, *P*-62*m*), a = 6.7055(4), c = 3.4028(3) Å, Z = 3						
Atom	Wyckoff position	Atomic coordinates				B_{iso} (Å^2)
		x	*y*	*z*		
Pd1	3*g*	0.2685(5)	0	1/2		0.71(4)
Pd2	3*f*	0.6095(5)	0	0		0.71(4)
Ge1	2*d*	1/3	2/3	1/2		0.32(9)
Ge2	1*a*	0	0	0		0.32(9)

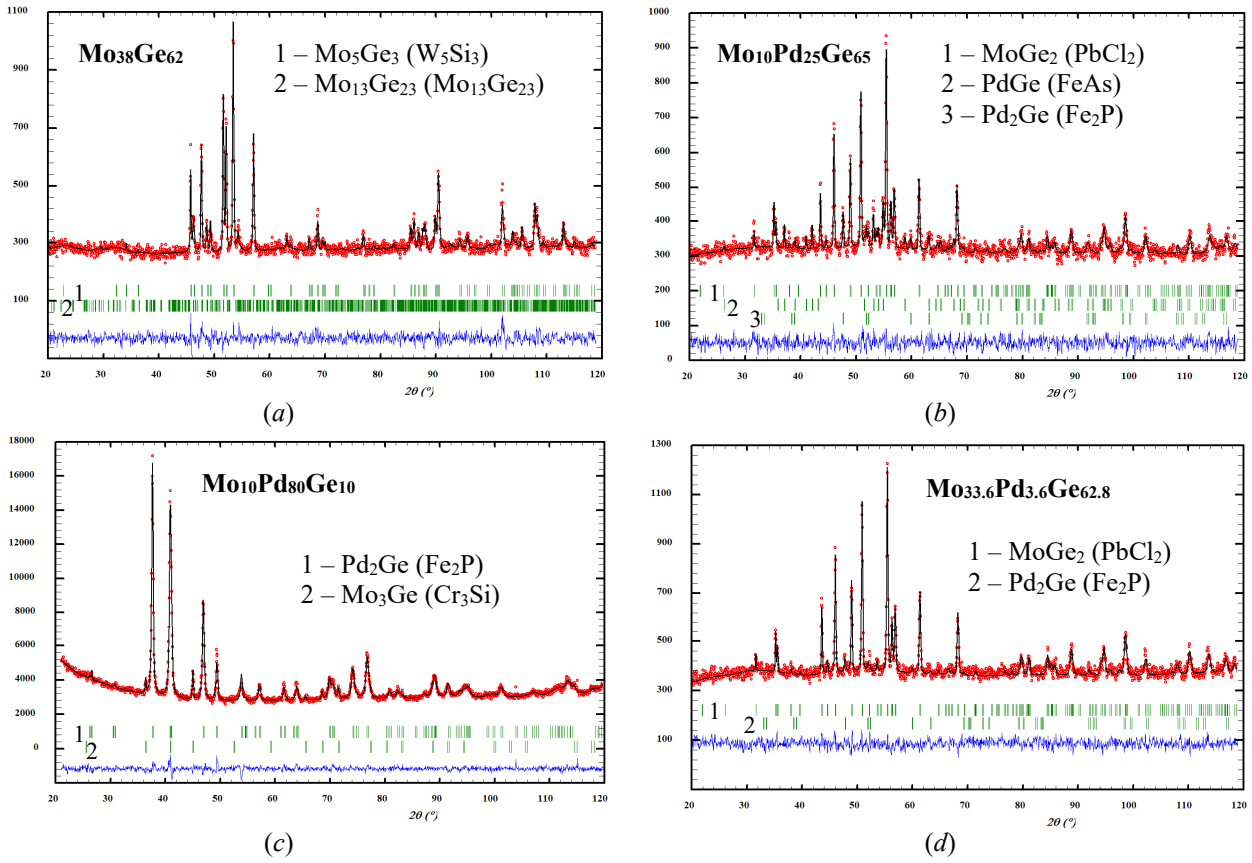

Fig. 4 Observed, calculated and difference (bottom) X-ray powder diffraction patterns for the $Mo_{38}Ge_{62}$ (*a*) (DRON-2.0 M diffractometer, Fe *K*α radiation), $Mo_{10}Pd_{25}Ge_{65}$ (*b*) (DRON-2.0 M diffractometer, Fe *K*α radiation), $Mo_{10}Pd_{80}Ge_{10}$ (*c*) (HZG-4a diffractometer, Cu *K*α radiation), and $Mo_{33.6}Pd_{3.6}Ge_{62.8}$ (*d*) (DRON-2.0 M diffractometer, Fe *K*α radiation) samples.

Table 5 Interatomic distances (δ) and coordination numbers (CN) in the structures of $(Mo_{0.87}Pd_{0.13})Ge_2$ phase (standard deviation < 0.005 Å).

Atoms		δ (Å)	Atoms		δ (Å)	Atoms		δ (Å)
Ge1	2Ge1	2.561	Ge2	$2(Mo_{0.87}Pd_{0.13})$	2.660	$(Mo_{0.87}Pd_{0.13})$	Ge1	2.575
(CN = 8)	$(Mo_{0.87}Pd_{0.13})$	2.575	(CN = 7)	$2(Mo_{0.87}Pd_{0.13})$	2.663	(CN = 9)	2Ge1	2.601
	$2(Mo_{0.87}Pd_{0.13})$	2.601		2Ge1	2.677		2Ge2	2.660
	2Ge2	2.677		$(Mo_{0.87}Pd_{0.13})$	2.886		2Ge2	2.663
	$(Mo_{0.87}Pd_{0.13})$	2.713					Ge1	2.713
							Ge2	2.886

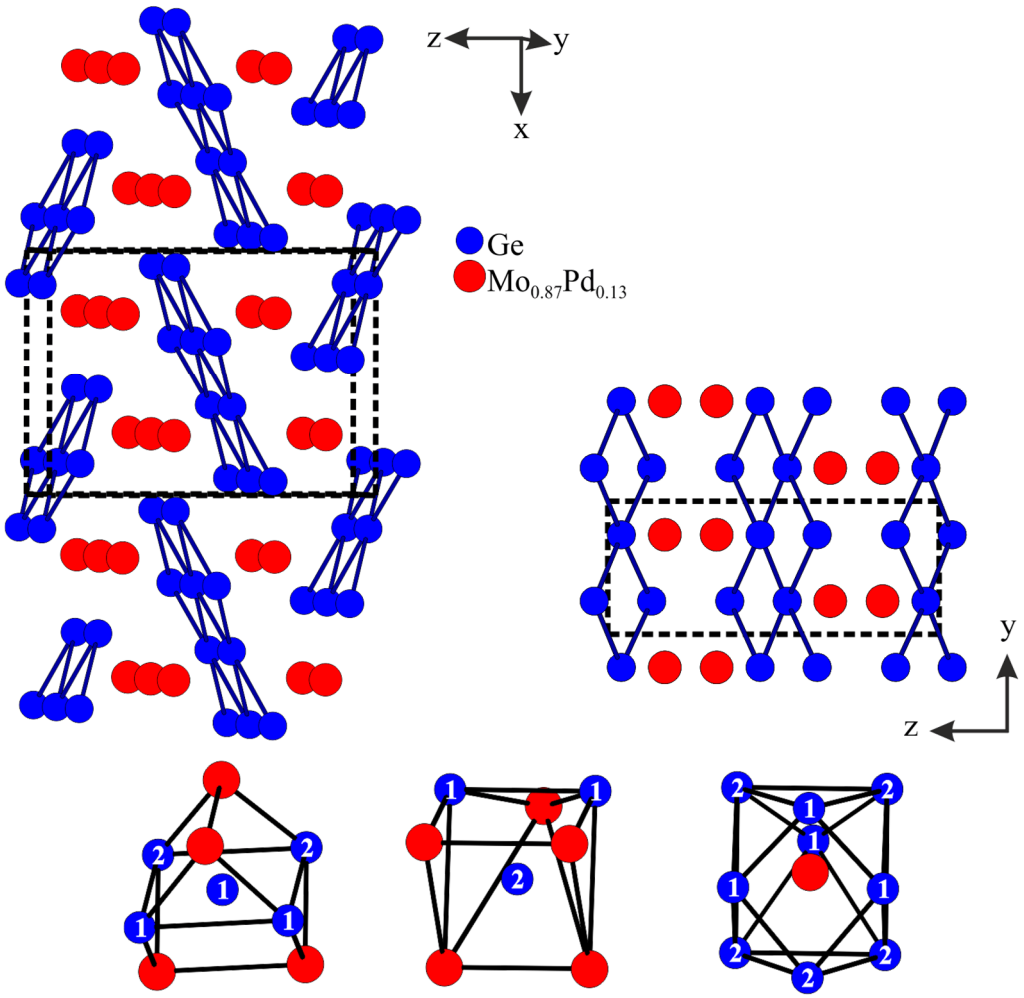

Fig. 5 Unit cell of the structures of the $(Mo_{0.87}Pd_{0.13})Ge_2$ phase and coordination polyhedra of the different atom sites.

Conclusions

We have constructed the isothermal cross-section of the phase diagram of the ternary Mo–Pd–Ge system at 600°C.

According to the results of the analysis by X-ray diffraction and energy-dispersive spectroscopy, the existence in the ternary system Mo–Pd–Ge of solid solutions of the binary compounds $MoGe_2$ (structure type $PbCl_2$, Pearson symbol *oP*12, space group *Pnma*, 6.5 at.% Pd), PdGe (FeAs, *oP*8, *Pnma*, 6.8 at.% Mo), compounds were established.

Solid solutions of palladium can also be qualified as catalysts with all the desired properties. We have confirmed solubility of palladium in the binary compound $MoGe_2$ up to 6.5 at.%, where Pd atoms substitute for Mo atoms. Calculations of the interatomic distances in $(Mo_{0.87}Pd_{0.13})Ge_2$ show that the shortest distance between atoms of the statistical mixture $(Mo_{0.87}Pd_{0.13})$ measures

3.445 Å. The shortest Pd-Pd distance in pure palladium is 2.751 Å [18]. It ensures greater isolation of the Pd atoms and formation of active centers. The solid solution $(Mo_{0.87}Pd_{0.13})Ge_2$ with a relatively small amount of palladium could show catalytic activity and selectivity in semi-hydrogenation reactions and decreases the cost cause by the noble metal.

Acknowledgement

This work was supported by the Ministry of Education and Science of Ukraine (grant No. 0121U109766).

N. Muts and Y. Tokaychuk are grateful to the program Presidential Discretionary-Ukraine Support Grants for financial support.

References

[1] E.M. Fiordaliso, I. Sharafutdinov, H.W.P. Carvalho, J. Kehres, J-D. Grunwaldt, I. Chorkendorff, C.D. Damsgaard, *Sci. Technol. Adv. Mater.* 20 (2019) 521-531. https://doi.org/10.1080/14686996.2019.1603886

[2] O. Matselko, R.R. Zimmermann, A. Ormeci, U. Burkhardt, R. Gladyshevskii, Yu. Grin, M. Armbrüster, *J. Phys. Chem.* 122 (2018) 21891-21896. https://doi.org/10.1021/acs.jpcc.8b05732

[3] P. Villars, K. Cenzual, J.L.C. Daams, F. Hulliger, H. Okamoto, K. Osaki, A. Prince, S. Iwata, *Pauling File, Inorganic materials database and design system. Binaries Edition , Crystal Impact. 2001*.

[4] A. Maldonado, K. Schubert, *Z. Metallkd.* 55 (1964) 619-626. https://doi.org/10.1515/ijmr-1964-551014

[5] E. Anderson, *J. Less-Common Met*. 6 (1964) 81-84. https://doi.org/10.1016/0022-5088(64)90009-8

[6] A. Searcy, R. Peavler, *J. Am. Chem. Soc.* 75 (1953) 5657-5659. https://doi.org/10.1021/ja01118a055

[7] A. Brown, *Nature (London)* 206 (1965) 502-503. https://doi.org/10.1038/206502a0

[8] H. Völlenkle, A. Preisinger, H. Nowotny, *Z. Kristallogr*. 124 (1967) 9-25. https://doi.org/10.1524/zkri.1967.124.16.9

[9] R. Dronskowski, A. Simon, *Z. Kristallogr.* 197 (1991) 131-135. https://doi.org/10.1524/zkri.1991.197.1-2.131

[10] R. Flükiger, J.A. Muller, *Solid State Commun*. 14 (1974) 443-447. https://doi.org/10.1016/0038-1098(74)90964-8

[11] H. Pfisterer, K. Schubert, *Z. Metallkd*. 41 (1950) 358-367. https://doi.org/10.1515/ijmr-1950-411009

[12] W. Wopersnow, K. Schubert, *J. Less-Common Met.* 52 (1977) 1-12. https://doi.org/10.1016/0022-5088(77)90230-2

[13] P. Matkovic, K. Schubert, W. Wopersnow, *J. Less-Common Met.* 56 (1977) 69-75. https://doi.org/10.1016/0022-5088(77)90219-3

[14] W. Wopersnow, K. Schubert, *J. Less-Common Met*. 41 (1975) 97-103. https://doi.org/10.1016/0022-5088(75)90097-1

[15] T. Matkovic, K. Schubert, *J. Less-Common Met*. 58 (1978) 1-6. https://doi.org/10.1016/0022-5088(78)90078-4

[16] K. Khalaff, K. Schubert, *Z. Metallkd*. 65 (1974) 379-382. https://doi.org/10.1515/ijmr-1974-650510

[17] J. Rodriguez-Carvajal, *Recent Developments of the Program FULLPROF*, Commission on Powder Diffraction (IUCr). Newsletter 26 (2001) 12-19.

[18] P. Villars, K. Cenzual (Eds.), *Pearson's Crystal Data. Crystal Structure Database for Inorganic Compounds*, Release 2021/22, ASM International, Materials Park (OH), 2021.